ACS APPLIED MATERIALS & INTERFACES

Research Article

www.acsami.org

Aqueously Dispersed Silver Nanoparticle-Decorated Boron Nitride Nanosheets for Reusable, Thermal Oxidation-Resistant Surface Enhanced Raman Spectroscopy (SERS) Devices

Yi Lin,*[,†] Christopher E. Bunker,*[,‡] K. A. Shiral Fernando,[§] and John W. Connell*[,⊥]

[†]National Institute of Aerospace, 100 Exploration Way, Hampton, Virginia 23666-6147,

[‡]Propulsion Directorate, Air Force Research Laboratory, Wright-Patterson Air Force Base, Ohio 45433-7103,

[§]Nanotechnology Group, University of Dayton Research Institute, Dayton, Ohio 45433-7103

[⊥]Mail Stop 226, Advanced Materials and Processing Branch, NASA Langley Research Center, Hampton, Virginia 23681-2199

Supporting Information

ABSTRACT: The impurity-free aqueous dispersions of boron nitride nanosheets (BNNS) allowed the facile preparation of silver (Ag) nanoparticle-decorated BNNS by chemical reduction of an Ag salt with hydrazine in the presence of BNNS. The resultant Ag−BNNS nanohybrids remained dispersed in water, allowing convenient subsequent solution processing. By using substrate transfer techniques, Ag−BNNS nanohybrid thin film coatings on quartz substrates were prepared and evaluated as reusable surface enhanced Raman spectroscopy (SERS) sensors that were robust against repeated solvent washing. In addition, because ofthe unique thermal oxidation-resistant properties of the BNNS, the sensor devices may be readily recycled by short-duration high temperature air oxidation to remove residual analyte molecules in repeated runs. The limiting factor associated with the thermal oxidation recycling process was the Ostwald ripening effect of Ag nanostructures.

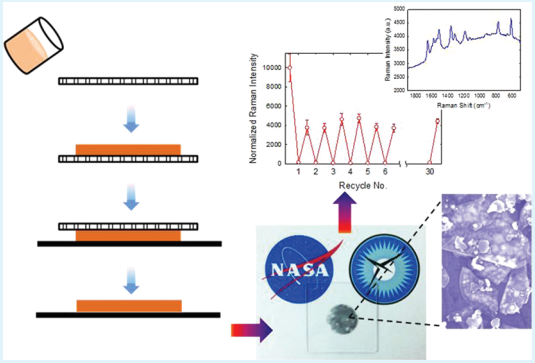

KEYWORDS: *boron nitride nanosheets, nanometal decoration, reusable, SERS, wet transfer*

INTRODUCTION

Surface-enhanced Raman spectroscopy (SERS) techniques are based on the Raman signal enhancement due to the surface plasmon of the noble metal nanoparticles [such as silver (Ag) and gold (Au)] and have been widely used for detection of trace organic and biological molecules.[1−4] The reproducibility of SERS results has always been a challenge due to various reasons such as uneven local hot spots of metal nanostructures. Reusable SERS devices are also highly desirable to lower the cost due to the use of noble metals and thus have attracted increasing attention. A few recycling techniques such as solvent wash[5−11] and UV cleaning[12−14] were reported. Thorough analyte removal is best achieved via thermal treatment in air (or thermal oxidation), which was only very recently explored on a SERS-active Au/Ag bilayer film with a protective alumina coating.[15]

Nanotubes, nanorods/nanowires, and nanosheets are often used as supports for nanoparticle decoration, forming hierarchical nanohybrids.[16−19] In these materials, the supporting substrates sometimes offer synergistic effects to the intrinsic properties of the nanoparticles, making the nanohybrids much more attractive in applications than the nanoparticles alone. For example, carbon nanotubes and graphene are excellent supports for palladium (Pd)-based heterogeneous catalysts in Suzuki reactions, with much improved activity than unsupported Pd catalysts.[20−22] Recently, Kamat and co-workers discussed in detail how graphene sheets may capture and "shuttle" electrons to the electrodes, resulting in enhanced photoelectrochemical and photocatalytic performance of graphene-supported titanium dioxide (TiO_2) nanoparticles and TiO_2 − noble metal dual nanoparticle systems.[19,23−25] In SERS measurements, the use of substrate supports (such as graphene[26−34]) also improves the local dispersion of the noble metal nanoparticles, resulting in enhancements of both sensitivity and signal reproducibility.

The exploration into the preparation and properties of hexagonal boron nitride nanosheets (BNNS) is in its infancy.[35−49] As the insulating structural analog of graphene, BNNS have a unique set of properties that have distinct similarities and differences compared to their carbon counterparts. For example, BNNS are similarly thermally conductive as graphene. While graphene has rich defect and conjugated carbon chemistry, BNNS are also expected to have rich chemistry, such as those based on Lewis acid−base interactions

Received: December 9, 2011
Accepted: January 26, 2012
Published: January 26, 2012

because of the locally highly polarized boron−nitrogen bonds.[40−42] Comparing to graphene, however, BNNS are expected to be much more inert against oxidation and withstand thermal treatment in air beyond 700 °C. Also, the large band-gap of BNNS makes them excellent transparent materials in the visible and near-IR regions.[40−44]

Although the decoration of BNNS with metal or metal oxide nanoparticles is essentially an unexplored area,[50] many strategies developed for the decoration of other nanomaterial supports, such as carbon nanotubes,[16−18] graphene,[19] and boron nitride nanotubes,[51−57] may be borrowed. For example, decorations of carbon nanotubes[16,17] and graphene with metal nanoparticles[19] can be achieved by chemically reducing metal salts in the presence of these carbon nanomaterials.

For potential applications, it is sometimes desirable that the nanomaterial supports and the resultant nanohybrids are in homogeneous dispersions for the convenience of solution processing. We recently reported the convenient preparation of impurity-free BNNS aqueous dispersions without the use of any organic functional groups or surfactants.[43] This procedure involved simply sonicating pristine hexagonal boron nitride (h-BN) powder in water followed by centrifugation to isolate the exfoliated BNNS with one or multiple atomic layers in the supernatant. The exfoliation and dispersion of BNNS was due to the combination of solvent polarity effect and the sonication-assisted hydrolysis of h-BN. The BNNS surface remained largely intact, with the presence of a small amount of hydroxyl groups located at dangling boron atoms as indicated by spectroscopic investigations. By taking advantage of the convenience in obtaining such BNNS aqueous dispersions, here we report a facile method to decorate these nanosheet surfaces with Ag nanoparticles in homogeneous aqueous environment at room temperature. The Ag−BNNS nanohybrids remained stable in the dispersions without the use of surfactants or additional functional groups. Subsequently, the impurity-free nanohybrid dispersions were readily processed, using simple substrate transfer techniques, into robust and reusable sensor devices for SERS with highly reproducible results. In particular, the thermal oxidation-resistant characteristics of BNNS allowed the fabricated Ag−BNNS SERS sensors to be recyclable in multiple air oxidation treatments without any reduced performance, except for the expected intensity drop during the first cycle.

EXPERIMENTAL SECTION

Materials. h-BN powder (size -10P, Lot HZ010PA4.$06) was provided by UK Abrasives. Silver acetate (99%), hydrazine hydrate (reagent grade, 50-60%), and rhodamine 6G (R6G, 99%) were purchased from Aldrich. Methylene chloride (certified ACS grade) was obtained from Fisher Scientific. All chemicals were used as received.

Measurements. Scanning electron microscopy (SEM) imaging, low-magnification transmission electron microscopy (TEM) imaging, and energy-dispersive X-ray (EDAX) mapping were carried out using a Hitachi S-5200 field-emission SEM system. High resolution TEM (HR-TEM) experiments were conducted on a JEOL 2100 field-emission TEM system. Optical absorption spectra were obtained using a Perkin-Elmer Lambda 900 UV/vis/NIR spectrometer. SERS spectra were acquired on a Thermo-Nicolet-Almega Dispersive Raman Spectrometer with 532 nm excitation. Each spectrum was accumulated with 16 1 s exposures at 20% laser power through a 25 μm pinhole.

BNNS Aqueous Dispersion. The pristine h-BN powder (200 mg) was sonicated in deionized water (100 mL) using a bath sonicator (Branson 2510, 40 kHz) for 16−24 h. The resultant slurry was centrifuged at ~3000 × g (IEC Clinical Centrifuge). The supernatant was passed through a coarse filter paper (Whatman cellulose), and the filtrate was collected as the aqueous dispersion of BNNS. The concentration of BNNS in the final dispersion was on the order of 0.05 mg/mL.

Ag−BNNS Nanohybrid Aqueous Dispersions. In a typical procedure to prepare a type I Ag−BNNS dispersion, an aqueous solution of hydrazine (2 mM, 1.25 mL) was mixed with a BNNS aqueous dispersion (~0.05 mg/mL, 1 mL). An aliquot of a silver acetate aqueous solution (10 mM, 0.25 mL) was then added to the mixture. Further aliquots of the salt solution were added at 10-min intervals until a total of 1 mL to reach completion of the reduction reaction at room temperature. The preparation of type II Ag−BNNS dispersions used the same starting solutions and followed the same procedure except for gradually adding five 0.25 mL aliquots of hydrazine solution into the BNNS−silver acetate solution mixture at room temperature.

RESULTS AND DISCUSSION

Aqueously Dispersed Ag−BNNS Nanohybrids. The aqueous BNNS dispersions were obtained in a procedure as previously described.[43] Decoration of BNNS with Ag nanoparticles was achieved by chemically reducing the corresponding metal salt precursor in the presence of BNNS in the aqueous dispersion. Hydrazine was selected as the reducing agent since it has been widely used in the preparation of free[58] or supported metal nanoparticles.[16−19] The room-temperature reaction started upon adding an aliquot of a silver acetate solution into the BNNS−hydrazine solution mixture. The colorless mixture gradually turned into light pink color within ~10 min, indicating the reduction of Ag^+ into metallic Ag nanoparticles by the hydrazine molecules. The color became more intense with further addition of aliquots of the salt solution into the mixture until the theoretically complete reaction was reached (hydrazine:Ag^+ = 1:4 mol/mol). The final pale pink-colored dispersion containing Ag nanoparticle-decorated BNNS (Figure 1 inset) appeared transparent and

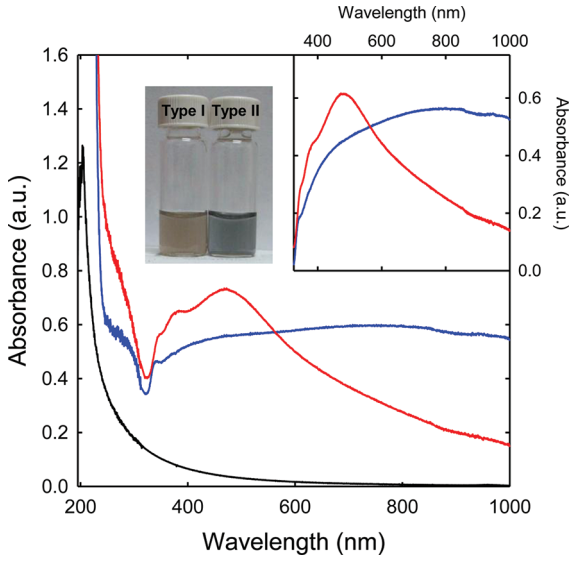

Figure 1. Optical absorption spectra and the corresponding photographs of type I (red) and type II (blue) Ag−BNNS nanohybrids in as-prepared aqueous dispersions. The spectrum of starting BNNS aqueous dispersion (diluted to the same equivalent BNNS concentration as in the Ag−BNNS dispersions) is also shown for comparison. Shown in the inset are the same spectra but subtracted with those of BNNS−hydrazine (type I) and BNNS−silver acetate (type II) starting solution mixtures, respectively, before the addition of the other reagent.

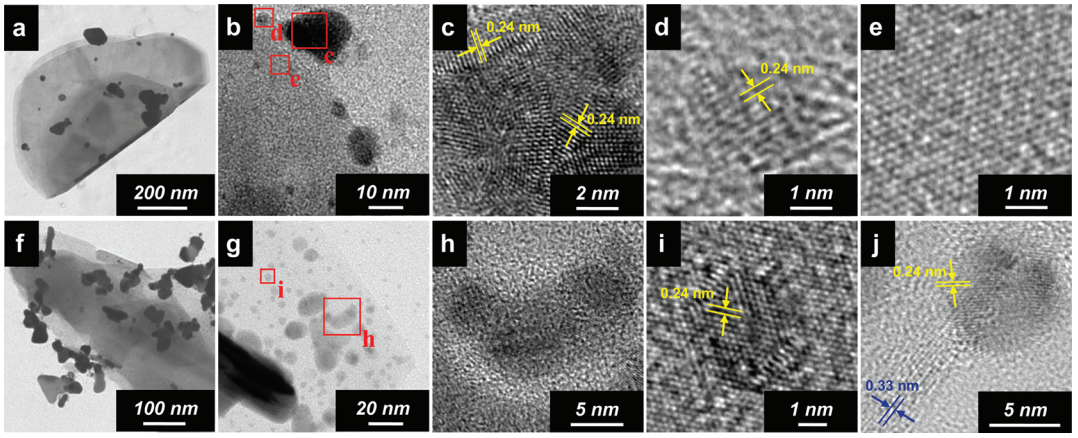

Figure 2. TEM images of (a–e) type I and (f–j) type II Ag–BNNS nanohybrids. Note that c–e are enlargement areas of the red squares in b, and h and i are enlargement areas of the red squares in g, respectively. (c, h) Polycrystalline Ag nanostructures. (d, i) sub-5 nm single-crystal Ag nanoparticles, (e, i) the hexagonal crystalline lattice of BNNS, (j) 6 nm polycrystalline Ag nanoparticle decorating at a folded edge of a 10-layered BNNS (~3 nm in thickness). Some Ag (111) and BN (002) lattice fringes (lattice distance ~0.24 and 0.33 nm, respectively) are highlighted in yellow and blue colors, respectively.

homogeneous, with no discernible precipitates. The optical absorption spectrum (Figure 1) exhibited a peak centered at ~470 nm, which is due to the well-known surface plasmon absorption of Ag nanoparticles.[59−62] The intensity of the plasmonic peak gradually increased during the course of reaction and reached a maximum after the addition of the last silver acetate aliquot (no further increase if more were added), indicating the completion of the reaction. In comparison, the spectrum of the essentially colorless BNNS dispersion had very low absorbance values (with a significant portion attributed to scattering effect).[43] By subtracting the absorption spectrum of the starting BNNS–hydrazine solution mixture, the plasmon peak of the BNNS-supported Ag nanostructures formed could be singled out (now at ~475 nm), which may provide a better comparison with data in the literature.[59−62] Although the band-gap peak of BNNS in the starting dispersion (~204 nm) was unambiguous, whether the attachment of Ag nanostructures affected the band-gap of BNNS was difficult to determine because the Ag nanostructures also exhibited multiple transitions in the nearby region as found in control experiments without the use of BNNS. Much detailed spectroscopic investigations or electronic measurements should provide further elucidation.

The order of reagent addition had an apparent impact on the characteristics of the resultant Ag nanostructures. Instead of adding silver acetate into the BNNS − hydrazine mixture solution as described above ("type I" Ag–BNNS), the addition of hydrazine into a BNNS − silver acetate solution mixture under otherwise the same conditions resulted in a pale blue solution (Figure 1 inset). The optical spectrum of this solution ("type II" Ag–BNNS) exhibited a very broad and featureless band extending across the visible and into the near-IR region (Figure 1). The spectral feature seemed to be quite similar to those attributed to the in-plane dipole plasmonic resonance of a distribution of Ag nanostructures of irregular and/or platelet shapes with different sizes, in addition to the significant scattering contribution.[59]

For TEM studies, a few drops of the two types of as-prepared Ag–BNNS dispersions were placed separately onto holey carbon-coated copper grids, followed by solvent evaporation. As shown in Figure 2, the Ag nanostructures in type I and type II Ag–BNNS products had different morphologies, which apparently caused their differences in the dispersion colors and the spectral shapes of the plasmonic bands. In type I Ag–BNNS, the BNNS surfaces were decorated with near-spherical Ag nanoparticles with diameters in the range of ~20–80 nm (Figure 2a–c). In contrast, type II Ag–BNNS contained BNNS-supported Ag nanostructures with rather irregular shapes in spite of similar dimensions (Figure 2f–h), consistent with the optical spectroscopy results. Both types of Ag nanoparticles were similarly polycrystalline in nature, with randomly orientated Ag^0 (111) and (200) phases (inter-lattice spacings ~0.24 and ~0.20 nm, respectively) (Figure 2c,h). In some cases, the Ag nanoparticles were seen attached to the folded edges of BNNS (Figure 2j), where the layered structures of BNNS (layer–layer distance ~0.33 nm) and the Ag lattices could be simultaneously identified. Importantly, most of the Ag nanostructures were found associated with BNNS, strongly suggesting that they were attached to the nanosheets during growth.

At high magnification in both samples, many BNNS-supported sub-5 nm Ag nanoparticles were also observed (Figure 2b, g). High-resolution imaging showed that these small Ag clusters were single crystals (Figure 2d, i) in comparison to the larger polycrystalline particles discussed above. This indicated that BNNS-supported Ag nanoparticle formation with either reagent addition sequence followed a seedling-templated growth process. It is likely that the sub-5 nm Ag nanoparticle "seeds" were formed either in the dispersion or directly on BNNS support when Ag^+ cations were in contact with hydrazine molecules. The BNNS in the dispersion then served as templates for the subsequent growth of the metallic Ag seed nanoparticles on their surfaces. The templating effect was more obvious for the nanoparticles formed at the nanosheet edges, where conformal ("flat") metal–BN interfaces (such as the example shown in Figure 2b) could be observed. The formation of Ag nanoparticles had little effect on the impurity-free BNNS supports, as the nanosheet surfaces retained the characteristic hexagonal crystalline lattice structures (Figure 2e, i).[43]

The different morphologies of Ag–BNNS nanohybrids from different reagent addition sequences were likely due to the kinetically controlled nature of the process since the reduction reaction and subsequent crystal growth occurred within

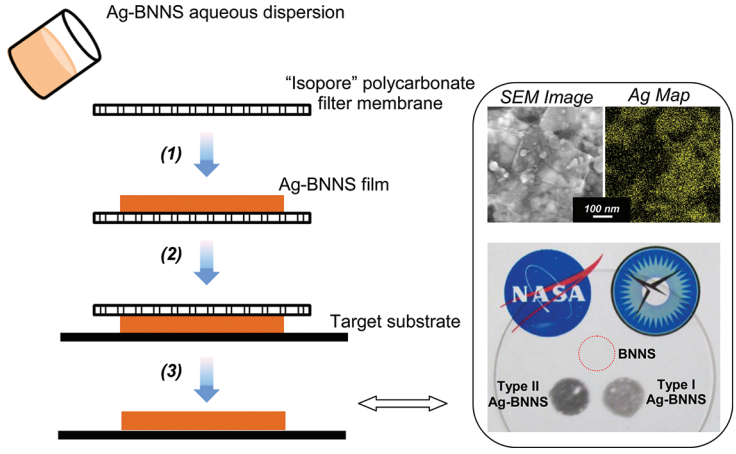

Figure 3. (Left) Cartoon schematic of the fabrication of Ag–BNNS-based SERS devices from straightforward vacuum filtration and wet transfer techniques: (1) filtration of an Ag–BNNS aqueous dispersion through a 0.1 μm polycarbonate filter membrane; (2) placement of the membrane-supported Ag–BNNS film face-down on the target substrate; (3) removal of the filter membrane in a methylene chloride bath followed by drying in nitrogen flow. (Right) Picture of several thin films supported on the same quartz substrate from the filtration-transfer procedure: plain BNNS (highlighted with a red circle), type I (lower colored film) and type II Ag–BNNS nanohybrids. Also shown on the right are an SEM image and the corresponding Ag map from EDAX measurement of a type II Ag–BNNS thin film transferred onto an Al SEM stub using the same technique.

minutes. In the preparation of type I Ag–BNNS (adding silver acetate to BNNS–hydrazine mixture), low local concentrations of Ag^+ near the nanosheet surfaces allowed for slower and thus more isotropic growth, forming near spherical nanoparticles. The growth was more anisotropic in the case of type II Ag–BNNS when more Ag^+ cations were available locally in a premixed BNNS–silver acetate dispersion. It is interesting to note that the type I Ag–BNNS aqueous dispersion was comparably much more stable than the type II nanohybrids. The former had little sediment formation over a 2–3 week period, whereas the latter exhibited significant precipitation overnight. This may be due to accelerated aggregation of BNNS-supported Ag nanostructures with anisotropic morphology. Another possible scenario was that the amine-affinitive nature of BNNS allowed the adsorption of some hydrazine molecules on the nanosheet surface via Lewis acid–base interactions[40–42] in type I nanohybrid preparation. This might have helped stronger anchoring of the nanoparticles on the dispersed nanosheets during seedling and growth and thus improved the stability of the resultant product in the dispersion. Nevertheless, the interactions between Ag and BNNS in both nanohybrid types were likely mostly van der Waals in nature with some ionic characteristics but with sufficient adhesion to remain attached after vigorous treatments such as sonication. Similar behavior has been observed with many metal–carbon nanotube or metal–graphene systems.[16–19]

Reusable Ag–BNNS SERS Devices. The relatively large lateral size of the BNNS supports (typically a few hundred nm to 1 μm) allowed the convenient and reproducible processing of the Ag–BNNS nanohybrid dispersions into thin film SERS devices via simple vacuum filtration and wet transfer techniques (Figure 3 left) that have been widely adopted in carbon nanoelectronics research.[63,64] In a typical experiment, a freshly prepared Ag–BNNS dispersion (1.5 mL) was filtered through a Millipore "Isopore" filter membrane (0.1 μm pore size). During the vacuum filtration, a PTFE O-ring (inner diameter = 0.9 cm or inner area = 0.64 cm^2) was placed on the filter membrane as a dispersion reservoir to confine the resultant coating area. Since the lateral sizes of BNNS were mostly over 100 nm, the polycarbonate filter membrane retained majority of the Ag–BNNS nanohybrid species from the dispersion. The collected thin film coating on the filter membrane was dried in nitrogen flow and then placed face-down onto a clean quartz substrate. The transfer of the Ag–BNNS thin film onto quartz was completed by removal of the polycarbonate-based filter membrane in a methylene chloride bath followed by repeated washing using the same solvent. After drying, dark-colored yet transparent Ag–BNNS nanohybrid thin films on the quartz substrate were obtained. The thin films from type II nanohybrids were visually darker in color than those from type I samples under similar conditions (Figure 3, right). In comparison, a similarly obtained plain BNNS thin film was of very low-color (highlighted by a red-colored dashed circle), consistent with the high optical transmission of BNNS in the visible region as demonstrated in previous reports.[39–45]

For SEM and EDAX analyses, the same wet transfer technique was applied except for using an aluminum SEM stub as the target substrate. An SEM image and the corresponding Ag mapping from EDAX of a type II Ag–BNNS sample are shown as examples in Figure 3. Majority of the nanosheets settled facially on the target substrate as a result of vacuum filtration-induced alignment.[43] Consistent with the TEM data in Figure 2, the BNNS-supported Ag nanoparticles were of rather irregular shapes and mostly tens of nm in diameter, with also the presence of some sub-5 nm species. At the given quantity of materials collected (from 1.5 mL of an as-prepared dispersion), the Ag–BNNS nanohybrids completely and uniformly covered the deposition area (~0.6 cm^2 considering the voids from air bubbles during transfer) on the substrate with 1-2 stacked layers of nanosheets. In comparison, smaller quantities of dispersions gave incomplete substrate coverage (see Figure S1 in the Supporting Information). Representative SEM images for a transferred type I Ag–BNNS sample (see Figure S2 in the Supporting Information) showed similar characteristics in the substrate coverage to those of type II samples, with the presence of near-spherical Ag nanoparticles consistent with the TEM observations in Figure 2.

R6G was used as the model compound for SERS sensing. In each experiment, a 10 μL drop of an ethanol solution of R6G

was placed on the thin film area of the sensor device and allowed to evaporate (typically spreading beyond the sensing material to reach a circular area with diameter of ~2 cm). Multiple SERS spectra (532 nm excitation, 16 1 s scans in each acquisition) were collected at different spots of the sample and averaged. As shown in Figure 4, well-resolved Raman signatures

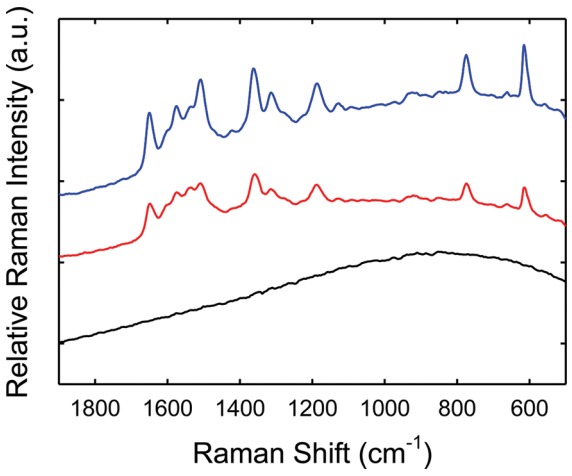

Figure 4. Averaged SERS spectra (532 nm excitation) of a R6G solution (1×10^{-5} M in ethanol) using devices fabricated from type I (red) and type II (blue) Ag–BNNS nanohybrid dispersions. The control spectrum of the same R6G solution deposited onto a blank BNNS film (black) is also shown for comparison. All spectra were offset for clarity.

of R6G at 1×10^{-5} M could be readily observed, while the same experiment with a blank BNNS film on quartz only yielded a strong yet featureless luminescence background. Apparently, the adsorption of R6G molecules on the Ag–BNNS nanohybrids enhanced the Raman response by orders of magnitude. The SERS enhancement factor (EF), using the equation $EF = I_{SERS}N_{bulk}/I_{Raman}N_{surface}$, was estimated to be on the order of 1×10^5 by comparing a SERS spectrum to the regular Raman spectrum of a bulk R6G sample (see Figure S3 in the Supporting Information). This value is comparable to a graphene-supported Ag system recently reported in the literature.[33]

It is worthwhile to mention that the SERS devices from the type II Ag–BNNS nanohybrids typically provided somewhat higher signal intensities than the analogous sensor prepared from the type I nanohybrids. Apparently, the morphological difference between these two types of nanohybrids with the same composition played a critical role. The fact that the nanohybrids with irregular Ag nanoparticle shapes were of better performance is consistent with the knowledge that anisotropic Ag structures often exhibit more SERS-active "hot spots".[59−62] The SERS spectral intensity may also be affected by the sizes of the BNNS-supported Ag nanoparticles, which were tuned by varying the concentrations of the starting salt and the corresponding hydrazine solutions (see Figure S4 in the Supporting Information). For example, it was found that the type II devices with larger nanoparticles (average ~50 nm) from higher starting reagent concentrations (10 mM silver acetate and 2 mM hydrazine) exhibited stronger SERS signals than those with smaller nanoparticle sizes (average <10 nm; from 1 mM silver acetate and 0.2 mM hydrazine), consistent with the known SERS-active size range for Ag.[1−4,39−42]

The Ag–BNNS SERS devices were robust against solvent washing and could be readily regenerated for repeated tests. Using a type II device as an example, the microscopic and nanoscopic morphology of a thin film surface transferred onto an aluminum stub (for SEM imaging) remained unchanged after extensive ethanol rinsing (see Figure S5 in the Supporting Information). As shown in Figure 5, the SERS response (by

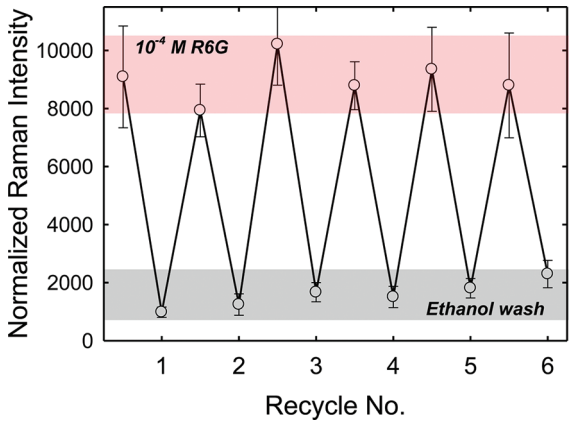

Figure 5. SERS responses (traced by the peak signal at 610 cm^{-1}) of a type II Ag–BNNS sensor device toward a R6G solution (1×10^{-4} M in ethanol) during repeated measurement-solvent washing cycles.

tracing the peak intensity at 610 cm^{-1}) of the same type II quartz device to a 1×10^{-4} M R6G ethanol solution remained consistent in six repeated measurement–ethanol washing cycles. It should be cautioned, however, that solvent washing could never be thorough as it always leaves a small amount of analyte residue due to physical adsorption. At 1×10^{-4} M R6G, the baseline intensity of the SERS device after solvent washing was typically 10–20% of the detected signal intensity (Figure 5), and the percentage may become even higher at lower initial analyte concentrations.

As previously mentioned, a unique advantage of BNNS as the supporting substrates for Ag nanoparticles is their resistance to thermal oxidation at high temperature. Under such conditions, the residual analyte molecules from previous runs may be completely removed with the supporting substrates (BNNS) remaining unaffected. Prolonged heating of the used Ag–BNNS sensor devices at 400 °C in air was shown to be sufficient to remove the organic residues as only a rather featureless and very low intensity spectral background was obtained in Raman measurement. However, the BNNS-attached Ag nanoparticles seemed to become "mobile" at or above this temperature with the formation of much larger spherical particles with much reduced SERS activity. For example, 1 h exposure of a SERS sensor in air resulted in large Ag particles with diameters of over 1 μm, while there was essentially no nanoparticle deposition on the surrounding intact BNNS surfaces (Figure 6a). Consequently, as shown in Figure 6d, the SERS signal intensity dropped to only ~10% of that observed with the non-treated devices after a mere 3 cycles of repeated long duration thermal oxidation (1 h in the first run and 30 min in the second and third runs), with very weak spectral peaks. Therefore, it was necessary to optimize the thermal oxidation regeneration by finding a balance between complete residue removal and retention of the SERS activity of the Ag nanostructures.

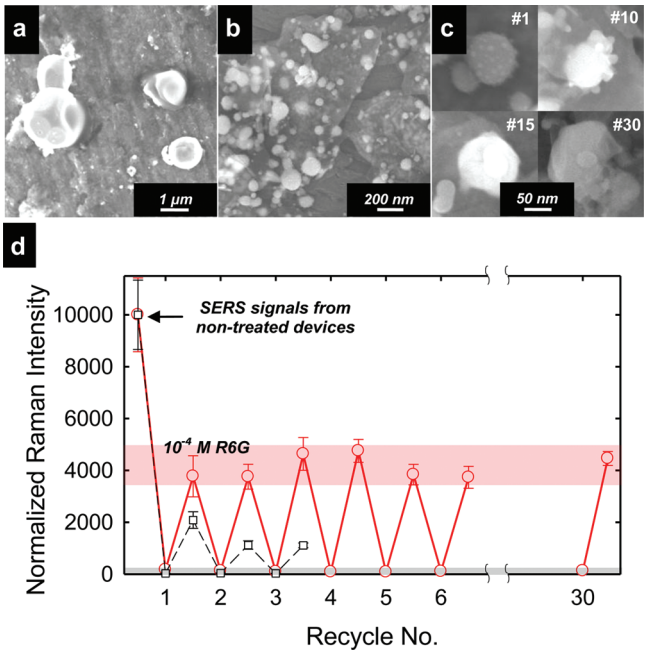

Figure 6. (a, b) SEM images of type II Ag–BNNS thin films on Al SEM stubs but subjected to long- (1 h) and short-duration (2 min) thermal oxidation treatment at 400 °C in air, respectively. (c) Morphology of individual Ag nanoparticles supported on BNNS after various cycles of 2 min treatments at 400 °C in air (the recycle number is indicated in each panel). (d) SERS responses (traced by the peak signal at 610 cm^{-1}) of two identical type II Ag–BNNS sensor devices toward a R6G solution (1×10^{-4} M in ethanol) during repeated measurement-thermal oxidation cycles. The red-colored symbols and solid line represent the cycles with each treatment carried out at 400 °C in air for 2 min. The black-colored symbols and dashed lines represent the cycles run at the same temperature but for much longer time period (1 h in the first cycle and 30 min in the second and third cycles).

To further investigate this phenomenon, a similarly prepared Ag–BNNS SERS device (type II) was exposed at 400 °C in air for 2 min. In contrast to the initially irregular-shaped Ag nanostructures before thermal oxidation, SEM images (Figure 6b) showed the formation of spherical Ag nanoparticles of similar dimensions (30–100 nm) within the reported SERS-active diameter region of Ag.[1−4,39−42] It is interesting to mention that these spherical Ag nanoparticles exhibited hierarchical nanostructures when closely examined, with multiple sub-5 nm nanoparticles decorating on the outer surface of the main metallic body (Figure 6c). This strongly indicated an ongoing Ostwald ripening process of Ag nanoparticles on BNNS supports, consistent with the observation of micrometer-sized particles with prolonged heating as shown in Figure 6a. However, in repeated 2 min thermal oxidation cycles, despite continuous morphological change to somewhat more sintered structures, there was only slight increase in the average diameter of the BNNS-supported Ag nanoparticles (Figure 6c). Apparently, both the short duration of the treatments and the BNNS supporting effect benefited the size retention of the Ag nanoparticles, with the intensive metal sintering observed in much longer thermal treatments kinetically not ready to occur.

The size stability of the Ag nanoparticles afforded the stable SERS performance of the Ag–BNNS device in such repeated treatments. As shown in Figure 5d, the SERS device after the first treatment at 400 °C for 2 min retained a reasonable response toward R6G with an absolute Raman intensity reduced to ~40% as compared to the untreated device. This reduction was expected as the Ag nanostructure went from more (irregular/platelet-shaped) to less SERS-active morphology (spherical-shaped). Nevertheless, the device thereafter exhibited consistent performance with additional repeated thermal treatments under the same conditions. With each cycle started with a "clean" baseline (no residual analyte from previous cycle), the SERS signals of R6G molecules showed no deterioration even after 30 cycles as conducted in the current report. Although the surfaces of Ag nanoparticles might have been partially oxidized after thermal oxidation treatments (see preliminary X-ray photoelectron spectroscopy (XPS) results in Figure S6 in the Supporting Information), the bulk nanoparticles remained metallic in nature with plasmonic resonance strong enough for retained SERS enhancement capabilities.

It should be acknowledged that there are other unique advantageous aspects of using BNNS as support of Ag nanoparticles for SERS sensors. For example, BNNS are known to have affinity for Lewis base compounds.[40−42] This characteristic may enable selective sensing of certain organic and biological molecules. In addition, unlike their carbon counterparts, the Raman signal of BNNS (E_{2g} peak typically at ~1365 cm^{-1})[40−43] is very weak and no enhancement by Ag decoration was observed; the reason for this is not clear. Nevertheless, BNNS provide low background interference in the SERS sensing and thus may enable spectral acquisition of higher resolution than the use of nanocarbon substrates. It is known that, when using carbon nanomaterials such as graphene as supports for noble metals, the G- and D-band signals in the region of 1200–1700 cm^{-1} are subjected to significant SERS enhancement and can thus strongly interfere with many analyte signals.[26−34] In a set of comparative experiments, graphene oxide (GO) in an aqueous dispersion was used as the substrate instead of BNNS for a similar SERS device by following the same preparation procedure as the type II Ag–BNNS sensors discussed above. It is apparent that the SERS spectrum was overwhelmed by the GO signals at a R6G concentration of 1×10^{-5} M (Figure S7). Furthermore, the SERS signals significantly diminished after the short term thermal oxidation treatments at 400 °C for 2 min, which is in sharp contrast with observed retention of signals when using Ag–BNNS devices (Figure 6).

CONCLUSIONS

Ag nanoparticle-decorated BNNS were prepared by reducing a silver salt using hydrazine in the presence of BNNS in aqueous dispersions at room temperature. It was shown that the reagent addition sequence affected the morphology and optical properties of the resultant Ag nanostructures. The Ag–BNNS nanohybrids in dispersions were conveniently processed into highly active quartz SERS devices via straightforward wet transfer techniques. The morphological difference of Ag nanostructures from the different reagent addition sequences had a distinguishable effect on the SERS performance of the resultant devices. Nevertheless, the SERS sensors fabricated from either addition sequence were robust against solvent washing. In addition, because of the thermal oxidation-resistant nature of BNNS substrates, the SERS devices were recyclable for as many as 30 times upon short-duration thermal treatments at 400 °C in air with essentially no decrease of performance despite an expected initial sensitivity drop from Ostwald

dx.doi.org/10.1021/am201747d | ACS Appl. Mater. Interfaces 2012, 4, 1110–1117

ripening of Ag nanostructures. Although further optimization is needed, the convenient fabrication and reusability of Ag–BNNS sensor devices may provide novel tools for low cost, reliable, quantitative, and selective SERS sensing. The reported methodology in the preparation of Ag–BNNS aqueous dispersions and the subsequent processing may also provide guidance to the exploration of other metal–BNNS nanohybrids systems for applications such as catalysis, sensing, and energy storage.

■ ASSOCIATED CONTENT

Supporting Information

SEM images showing the substrate coverage of type II Ag–BNNS thin film samples, SEM images of a type I Ag–BNNS thin film sample, SERS and Raman spectra of R6G for SERS-EF estimation, TEM images of type II Ag–BNNS samples with various Ag nanoparticle sizes and the SERS spectra from the corresponding devices, SEM images of a type II Ag–BNNS sample before and after prolonged ethanol rinsing, XPS data of type II Ag–BNNS devices with and without thermal treatments, and SERS/Raman spectra of a type II Ag-GO device for detection of R6G. This material is available free of charge via the Internet at http://pubs.acs.org.

■ AUTHOR INFORMATION

Corresponding Author

*E-mail: yi.lin-1@nasa.gov (Y.L.); christopher.bunker@wpafb.af.mil (C.E.B.); john.w.connell@nasa.gov (J.W.C).

Notes

The authors declare no competing financial interest.

■ ACKNOWLEDGMENTS

We thank Dr. W. Cao and Prof. H. Elsayed-Ali at the Applied Research Center of Old Dominion University for HR-TEM measurements, Prof. F. Gupton and K. Woodberry at Virginia Commonwealth University for XPS measurements, and T.V. Williams, an intern of the Langley Research Summer Scholars (LARSS) Program, for experimental assistance.

■ REFERENCES

(1) Campion, A.; Kambhampati, P. *Chem. Soc. Rev.* **1998**, *27*, 241.
(2) Kneipp, K.; Kneipp, H.; Itzkan, I.; Dasari, R. R.; Feld, M. S. *Chem. Rev.* **1999**, *99*, 2957.
(3) Ko, H.; Singamaneni, S.; Tsukruk, V. V. *Small* **2008**, *4*, 1576.
(4) Special Issue on SERS: *Chem. Soc. Rev.* **2008**, *37*.
(5) Yonzon, C. R.; Haynes, C. L.; Zhang, X. Y.; Walsh, J. T.; Van Duyne, R. P. *Anal. Chem.* **2004**, *76*, 78.
(6) Sackmann, M.; Bom, S.; Balster, T.; Materny, A. *J. Raman Spectrosc.* **2007**, *38*, 277.
(7) Bantz, K. C.; Haynes, C. L. *Vib. Spectrosc.* **2009**, *50*, 29.
(8) Aldeanueva-Potel, P.; Faoucher, E.; Alvarez-Puebla, R. A.; Liz-Marzan, L. M.; Brust, M. *Anal. Chem.* **2009**, *81*, 9233.
(9) Li, D.; Li, D.-W.; Li, Y.; Fossey, J. S.; Long, Y.-T. *J. Mater. Chem.* **2010**, *20*, 3688.
(10) Hwang, J.-S.; Chen, K.-Y.; Hong, S.-J.; Chen, S.-W.; Syu, W.-S.; Kuo, C.-W.; Syu, W.-Y.; Lin, T.-Y.; Chiang, H.-P.; Chattopadhyay, S.; Chen, K.-H.; Chen, L.-C. *Nanotechnology* **2010**, *21*, 025502.
(11) Lv, B.; Xu, Y.; Tian, H.; Wu, D.; Sun, Y. *J. Solid State Chem.* **2010**, *183*, 2968.
(12) Li, X.; Chen, G.; Yang, L.; Jin, Z.; Liu, J. *Adv. Funct. Mater.* **2010**, *20*, 2815.
(13) Sadate, S.; Calzzani, F.; Kassu, A.; Sharma, A.; Ruffin, P.; Brantley, C.; Edwardds, E. *Opt. Eng.* **2010**, *49*, 106501.
(14) Sinha, G.; Depero, L. E.; Alessandri, I. *ACS Appl. Mater. Interfaces* **2011**, *3*, 2557.
(15) Mahurin, S. M.; John, J.; Sepaniak, M. J.; Dai, S. *Appl. Spectrosc.* **2011**, *65*, 417.
(16) Wildgoose, G. G.; Banks, C. E.; Compton, R. G. *Small* **2006**, *2*, 182.
(17) Georgakilas, V.; Gournis, D.; Tzitzios, V.; Pasquato, L.; Guldi, D.; Prato, M. *J. Mater. Chem.* **2007**, *17*, 2679.
(18) Kolmakov, A.; Chen, X.; Moskovits, M. *J. Nanosci. Nanotechnol.* **2008**, *8*, 111.
(19) Kamat, P. V. *J. Phys. Chem. Lett.* **2010**, *1*, 520.
(20) Corma, A.; Garcia, H.; Leyva, A. *J. Mol. Catal. A: Chem.* **2005**, *230*, 97.
(21) Scheuermann, G. M.; Rumi, L.; Steurer, P.; Bannwarth, W.; Mulhaupt, R. *J. Am. Chem. Soc.* **2009**, *131*, 8262.
(22) Siamaki, A. R.; Khder, A. E. R. S.; Abdelsayed, V.; El-Shall, M. S.; Gupton, B. F. *J. Catal.* **2011**, *279*, 1.
(23) Williams, G.; Brian, S.; Kamat, P. V. *ACS Nano* **2008**, *2*, 1487.
(24) Lightcap, I. V.; Kosel, T. H.; Kamat, P. V. *Nano Lett.* **2010**, *10*, 577.
(25) Ng., Y. H.; Lightcap, I. V.; Goodwin, K.; Matsumura, M.; Kamat, P. V. *J. Phys. Chem. Lett.* **2010**, *1*, 2222.
(26) Xu, C.; Wang, X. *Small* **2009**, *5*, 2212.
(27) Goncalves, G.; Marques, P. A. A. P.; Granadeiro, C. M.; Nogueira, H. I. S.; Singh, M. K.; Gracio, J. *Chem. Mater.* **2009**, *21*, 4796.
(28) Rout, C. S.; Kumar, A.; Xiong, G.; Irudayaraj, J.; Fisher, T. S. *Appl. Phys. Lett.* **2010**, *97*, 133108.
(29) Wang, Y.; Ni, Z.; Hu, H.; Hao, Y.; Wong, C. P.; Yu, T.; Thong, J. T. L.; Shen, Z. X. *Appl. Phys. Lett.* **2010**, *97*, 163111.
(30) Huang, J.; Zhang, L.; Chen, B.; Ji, N.; Chen, F.; Zhang, Y.; Zhang, Z. *Nanoscale* **2010**, *2*, 2733.
(31) Polavarapu, L.; Manga, K. K.; Yu, K.; Ang, P. K.; Cao, H. D.; Balapanuru, J.; Loh, K. P.; Xu, Q.-H. *Nanoscale* **2011**, *3*, 2268.
(32) Zhang, Z.; Xu, F.; Yang, W.; Guo, M.; Wang, X.; Zhang, B.; Tang, J. *Chem. Commun.* **2011**, *47*, 6440.
(33) Liu, X.; Cao, L.; Song, W.; Ai, K.; Lu, L. *ACS Appl. Mater. Interfaces* **2011**, *3*, 2944.
(34) Ren, W.; Fang, Y.; Wang, E. *ACS Nano* **2011**, *5*, 6425.
(35) Corso, M.; Auwarter, W.; Muntwiler, M.; Tamai, A.; Greber, T.; Osterwalder, J. *Science* **2004**, *303*, 217.
(36) Novoselov, K. S.; Jiang, D.; Schedin, F.; Booth, T. J.; Khotkevich, V. V.; Morozov, S. V.; Geim, A. K. *Proc. Natl. Acad. Sci.* **2005**, *102*, 10451–10453.
(37) Pacile, D.; Meyer, J. C.; Girit, C. O.; Zettl, A. *Appl. Phys. Lett.* **2008**, *92*, 133107.
(38) Han, W.-Q.; Wu, L.; Zhu, Y.; Watanabe, K.; Taniguchi, T. *Appl. Phys. Lett.* **2008**, *93*, 223103.
(39) Zhi, C.; Bando, Y.; Tang, C.; Kuwahara, H.; Golberg, D. *Adv. Mater.* **2009**, *21*, 2889.
(40) Lin, Y.; Williams, T. V.; Connell, J. W. *J. Phys. Chem. Lett.* **2010**, *1*, 277.
(41) Nag, A.; Raidongia, K.; Hembram, K. P. S. S.; Datta, R.; Waghmare, U. V.; Rao, C. N. R. *ACS Nano* **2010**, *4*, 1539.
(42) Lin, Y.; Williams, T. V.; Cao, W.; Elsayed-Ali, H. E.; Connell, J. W. *J. Phys. Chem. C* **2010**, *114*, 17434.
(43) Lin, Y.; Williams, T. V.; Xu, T.-B.; Cao, W.; Elsayed-Ali, H. E.; Connell, J. W. *J. Phys. Chem. C* **2011**, *115*, 2679.
(44) Coleman, J. N.; Lotya, M.; O'Neill, A.; Bergin, S. D.; King, P. J.; Khan, U.; Young, K.; Gaucher, A.; De., S.; Smith, R. J.; Shvets, I. V.; Arora, S. K.; Stanton, G.; Kim, H.-Y.; Lee, K.; Kim, G. T.; Duesberg, G. S.; Hallam, T.; Boland, J. J.; Wang, J. J.; Donegan, J. F.; Grunlan, J. C.; Moriarty, G.; Shmeliov, A.; Nicholls, R. J.; Perkins, J. M.; Grieveson, E. M.; Theuwissen, K.; McComb, D. W.; Nellist, P. D.; Nicolosi, V. *Science* **2011**, *331*, 568.
(45) Wang, Y.; Shi, Z.; Yin, J. *J. Mater. Chem.* **2011**, *21*, 11371.
(46) Song, L.; Ci, L.; Lu, H.; Sorokin, P. B.; Jin, C.; Ni, J.; Kvashnin, A. G.; Kvashnin, D. G.; Lou, J.; Yakobson, B. I.; Ajayan, P. M. *Nano Lett.* **2010**, *10*, 3209.

(47) Shi, Y.; Hamsen, C.; Jia, X.; Kim, K. K.; Reina, A.; Hofmann, M.; Hsu, A. L.; Zhang, K.; Li, H.; Juang, Z.-Y.; Dresselhaus, M. S.; Li, L.-J.; Kong, J. *Nano Lett.* **2010**, *10*, 4134.
(48) Zeng, H.; Zhi, C.; Zhang, Z.; Wei, X.; Wang, X.; Guo, W.; Bando, Y.; Golberg, D. *Nano Lett.* **2010**, *10*, 5049.
(49) Erickson, K. J.; Gibb, A. L.; Sinitskii, A.; Rousseas, M.; Alem, N.; Tour, J. M.; Zettl, A. K. *Nano Lett.* **2011**, *11*, 3221.
(50) Wang, L.; Sun, C.; Xu, L.; Qian, Y. *Catal. Sci. Technol.* **2011**, *1*, 1119.
(51) Han, W.-Q.; Zettl, A. *J. Am. Chem. Soc.* **2003**, *125*, 2062.
(52) Sainsbury, T.; Ikuno, T.; Okawa, D.; Pacile, D.; Frechet, J. M. J.; Zettl, A. *J. Phys. Chem. C* **2007**, *111*, 12992.
(53) Huang, Q.; Bando, Y.; Zhao, L.; Zhi, C.; Golberg, D. *Nanotechnology* **2009**, *20*, 415501.
(54) Tang, C.; Li, J.; Bando, Y.; Zhi, C.; Goberg, D. *Chem. Asian J.* **2010**, *5*, 1220.
(55) Huang, Y.; Lin, J.; Bando, Y.; Tang, C.; Zhi, C.; Shi, Y.; Takayama-Muromachi, E.; Goberg, D. *J. Mater. Chem.* **2010**, *20*, 1007.
(56) Gao, Z.; Sawada, T.; Zhi, C.; Bando, Y.; Goberg, D.; Serizawa, T. *Soft Mater.* **2011**, *7*, 8753.
(57) Chen, R.; Zhi, C.; Yang, H.; Bando, Y.; Zhang, Z.; Sugiur, N.; Golberg, D. *J. Colloid Interf. Sci.* **2011**, *359*, 261.
(58) Cushing, B. L.; Kolesnichenko, V. L.; O'Connor, C. J. *Chem. Rev.* **2004**, *104*, 3893.
(59) Zhang, J.; Li, X.; Sun, X.; Li, Y. *J. Phys. Chem. B* **2005**, *109*, 12544.
(60) Orendorff, C. J.; Gearheart, L.; Jana, N. R.; Murphy, C. J. *Phys. Chem. Chem. Phys.* **2006**, *8*, 165.
(61) Jana, N. R.; Pal, T. *Adv. Mater.* **2007**, *19*, 1761.
(62) Lu, L.; Kobayashi, A.; Tawa, K.; Ozaki, Y. *Chem. Mater.* **2006**, *18*, 4894.
(63) Liu, Z.; Jiao, L.; Yao, Y.; Xian, X.; Zhang, J. *Adv. Mater.* **2010**, *22*, 2285.
(64) Li, X.; Zhu, Y.; Cai, W.; Borysiak, M.; Han, B.; Chen, D.; Piner, R. D.; Colombo, L.; Ruoff, R. S. *Nano Lett.* **2009**, *9*, 4359.